Long-term development of short-period gravity waves in middle Europe

D. Offermann,[1] J. Wintel,[1] C. Kalicinsky,[1] P. Knieling,[1] R. Koppmann,[1] and W. Steinbrecht[2]

Received 22 December 2010; revised 21 April 2011; accepted 26 April 2011; published 23 July 2011.

[1] The long-term development of short-period gravity waves is investigated using the analysis of temperature fluctuations in the mesosphere. The temperature fluctuations are quantified by their standard deviations σ based on data from OH measurements at Wuppertal (51°N, 7°E) and Hohenpeissenberg (48°N, 11°E) obtained from 1994 to 2009 at 87 km altitude. The temperatures are Fourier analyzed in the spectral regime of periods between 3 and 10 min. The resulting oscillation amplitudes correlate very well with the standard deviations. Shortest periods are taken as "ripples" that are indicative of atmospheric instabilities/breaking gravity waves. In consequence the standard deviations are used as proxies for gravity wave activity and dissipation. This data set is analyzed for seasonal, intradecadal, and interdecadal (trend) variations. Seasonal changes show a double peak structure with maxima occurring slightly before circulation turnaround in spring and autumn. This is found to be in close agreement with seasonal variations of turbulent eddy coefficients obtained from WACCM 3.5. The intradecadal variations show close correlations with the zonal wind and the annual amplitude of the mesopause temperature. The long-term trend (16 years) indicates an increase of gravity wave activity of 1.5% per year. Correspondences with dynamical parameters such as zonal wind speed and summer length are discussed.

Citation: Offermann, D., J. Wintel, C. Kalicinsky, P. Knieling, R. Koppmann, and W. Steinbrecht (2011), Long-term development of short-period gravity waves in middle Europe, *J. Geophys. Res.*, *116*, D00P07, doi:10.1029/2010JD015544.

1. Introduction

[2] Atmospheric gravity waves (GW) are known to be important parts of middle atmosphere dynamics. They have been intensively studied since the early work of Colin Hines [*Hines*, 1960] with respect to their influences on atmospheric structure and variability [e.g., *Andrews et al.*, 1987; *Fritts and Alexander*, 2003]. They are known to control the mesospheric circulation and its changes by dissipation and momentum deposition [e.g., *Fritts et al.*, 2006]. An extensive review on the voluminous literature on GW has been given by *Fritts and Alexander* [2003]. More recent developments are described e.g., by *Preusse et al.* [2006, 2008, 2009], *Ern et al.* [2004], *Jacobi et al.* [2006], *Krebsbach and Preuße* [2007], *Wu et al.* [2006], and the references given therein.

[3] Substantial amount of work has been spent on the question as to the origin of gravity waves in the mesosphere. There are many sources in the lower atmosphere (orographic structures, weather systems), and GW upward propagation in the middle atmosphere up to the mesopause has been extensively studied e.g., by ray tracing methods [*Preusse et al.*, 2009, and references therein]. Gravity waves are subject to many influences and modifications on their way up to the mesosphere and lower thermosphere, as for instance by wind filtering in the middle atmosphere [e.g., *Alexander*, 1998]. Wavelike oscillations are also known to be excited in situ in the mesosphere by breaking gravity waves and Kelvin-Helmholtz or convective instabilities. These have exceptionally short periods and wavelengths ("ripples"), and are investigated in detail by theory and imaging experiments [e.g., *Nakamura et al.*, 1999; *Horinouchi et al.*, 2002; *Hecht*, 2004, *Hecht et al.*, 2005, 2007; *Taylor et al.*, 1997, 2007; *Shiokawa et al.*, 2009]. Gravity wave–fine structure interactions, related Kelvin-Helmholtz instabilities, and turbulence production have also been numerically studied by *Fritts et al.* [2009, and references therein].

[4] Gravity wave amplitudes in the upper mesosphere are comparatively large. At the mesopause they appear to be the strongest of all types of waves (in temperature [*Offermann et al.*, 2009]). In the lower mesosphere and upper stratosphere their amplitudes are relatively small indicating considerable wave dissipation. Gravity waves therefore appear to be linked to turbulence production and hence to eddy diffusion in the mesosphere [e.g., *Rapp et al.*, 2004].

[5] Considering the general importance of gravity waves it is interesting to study possible long-term changes. Seasonal variations have been analyzed on many occasions, and sometimes with quite different results. Annual and

[1]Physics Department, Wuppertal University, Wuppertal, Germany.
[2]Meteorologisches Observatorium, Hohenpeissenberg, Germany.

0148-0227/11/2010JD015544

Table 1. List of Acronyms

Acronym	Definition
AMSU	Advanced Microwave Sounding Unit
AURA	NASA satellite, Earth science Projects Division
CRISTA	Cryogenic Infrared Spectrometers and Telescopes for the Atmosphere
DOY	Day Of Year
ESD	Equivalent Summer Duration
FFT	Fast Fourier Transform
GCM	General Circulation Model
GRIPS	Ground based Infrared P-branch Spectrometer
HIRDLS	High Resolution Dynamics Limb Sounder
LIMS	Limb Infrared Monitor of the Stratosphere
MLS	Microwave Limb Sounder
SABER	Sounding of the Atmosphere using Broadband Emission Radiometry
TIMED	Thermosphere, Ionosphere, Mesosphere, Energetics, and Dynamics
WACCM	Whole Atmosphere Community Climate Model

semiannual variations have been found with maxima at solstices or at equinox. The structures depend on the wave frequency, and can be different for different latitudes as well as different altitudes. Measurement parameter (wind, temperature) also appears to play a role. For details, see, e.g., *Manson et al.* [1999], *Jacobi et al.* [2006], *Dowdy et al.* [2007], *Offermann et al.* [2009], and *Preusse et al.* [2009], and the many references given therein. Interannual (intradecadal) and interdecadal (long-term trend) results are much more scarce. Considerable interannual variability has been observed, and there appear to be indications of solar cycle influences [e.g., *Jiang et al.*, 2006; *Jacobi et al.*, 2006]. An analysis of a limited data set at the station of Wuppertal (51°N, 7°E) was given by *Offermann et al.* [2006]. The latter data are substantially extended and analyzed in detail in the present paper.

[6] Gravity waves are extremely manifold as their wavelengths, periods, and propagation directions are considered. All these parameters vary with altitude, latitude, and specific location of the measurements. Data interpretation is therefore not easy, and a consistent climatology is obviously difficult to obtain. Furthermore ground based measurements lack horizontal and sometimes also vertical information. Satellite measurements are limited to gravity waves of longer wavelengths in the horizontal or vertical direction because of limited spatial resolution of limb sounders in the horizontal and nadir sounders in the vertical [e.g., *Alexander*, 1998; *McLandress et al.*, 2000; *Preusse et al.*, 2006]. These types of measurements have been performed by various satellites instruments such as MLS, LIMS, CRISTA, SABER, HIRDLS, and AMSU [*Wu and Waters*, 1996; *Fetzer and Gille*, 1994; *Eckermann and Preusse*, 1999; *Preusse et al.*, 2006, *Alexander and Ortland*, 2010; *Jiang et al.*, 2006]. (Explanation of the acronyms is given in Table 1.)

[7] Up to now the time intervals covered by satellite measurement series are rather limited. Much longer data series are available from various ground experiments. These include radar wind measurements, Lidar intensity or temperature measurements, and airglow spectral or imaging observations of temperature or intensity [e.g., *Fritts and Alexander*, 2003; *Scheer et al.*, 2006; *Jacobi et al.*, 2006; *Hoffmann et al.*, 2011, and references therein]. High time resolution can be obtained by these techniques. Particularly high resolution has been obtained by the OH technique. Mesospheric oscillations with periods of a few minutes have been observed by OH imaging experiments [e.g., *Taylor et al.*, 2007; *Hecht et al.*, 2007].

[8] In the present paper we discuss an OH data series covering 16 years of observation (1994–2009) with a time resolution of 1.3 min taken at the station of Wuppertal (51°N, 7°E, GRIPS II instrument). In addition, six years of data taken at Hohenpeissenberg (48°N, 11°E, GRIPS I, 2004–2009) are also included. This is a large amount of data, only part of which can be discussed here. The paper is organized as follows: Section 2 describes the data and their analysis. Section 3 compares oscillation amplitudes and the standard deviations σ_N from the nightly mean temperature as a proxy for mesospheric waves. In section 4 the seasonal variations of this parameter are discussed. This includes wave breaking and eddy coefficients K_{zz} as obtained from a recent atmospheric model WACCM 3.5. Section 5 analyzes intradecadal and interdecadal variations. Section 6 discusses the results and compares them with other data. Section 7 summarizes the results.

2. Data and Analysis

[9] The hydroxyl (OH) layer in the upper mesosphere is centered at about 87 km altitude and is 8 km wide (full width at half maximum) [e.g., *Bittner et al.*, 2002; *Oberheide et al.*, 2006; *Mulligan et al.*, 2009; *Offermann et al.*, 2010]. The exact layer altitude is not very important for the wave analyses presented here. The OH molecules are chemically excited and emit a broad spectrum of lines at visible and near infrared wavelengths. These emissions are widely used to determine atmospheric temperatures at this altitude [e.g., *Scheer et al.*, 2006]. Such measurements are also taken at the station of Wuppertal (51°N, 7°E) by a small grating spectrometer of moderate resolution (GRIPS II). With this instrument the intensities of three P band lines at wavelengths of 1.524 μm, 1.533 μm, and 1.543 μm are measured, from which the temperature is derived. Instrument and measurement technique are described in detail by *Bittner et al.* [2002] and *Offermann et al.* [2010]. A similar ("twin") instrument (GRIPS I) is operated at the station of Hohenpeissenberg (48°N, 11°E) about 360 km south of Wuppertal [*Offermann et al.*, 2010, 2011]. The measurements are taken during night to avoid stray light from the sun. The fields of view are tilted northward to avoid moon interferences. Cloud-free observations were used only. The three infrared lines of one spectrum are measured within 54 s. This should be fast enough to limit the distortion of the derived temperature value by haze possibly drifting into the field of view.

[10] The OH temperatures show strong variations on a wide range of time scales, reaching from minutes to decades. One recurrent variation with large amplitude is the seasonal change. An example for Wuppertal is shown in Figure 1. Mean nightly temperatures are given. They are low in summer and high in winter which is due to the large scale circulation. The seasonal variation is modeled by an harmonic analysis (solid line in Figure 1) with seven free parameters: mean temperature T_0, three amplitudes A_1,A_2, A_3 for annual, semiannual, and terannual components, and the corresponding phases. Figure 1 shows the data of 2005.

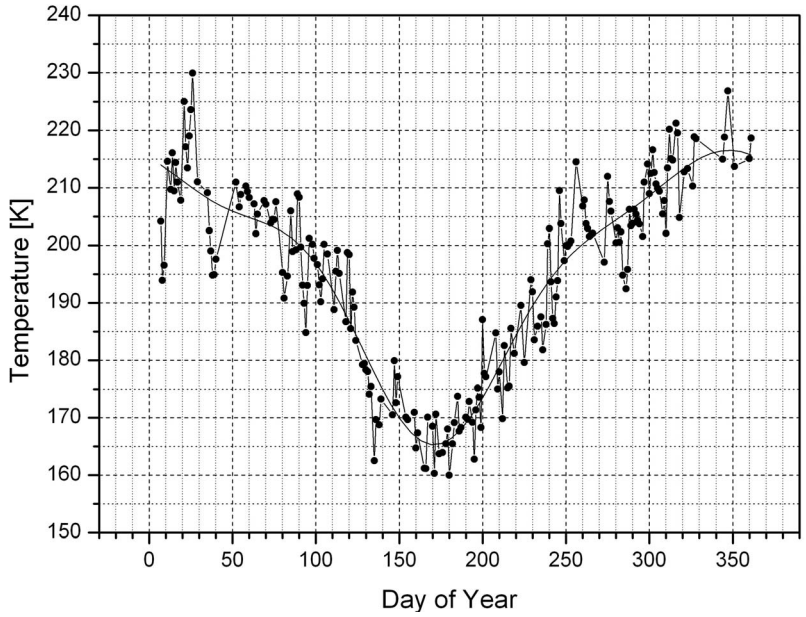

Figure 1. Seasonal variation of OH temperatures in 2005. Nightly mean values are given. The solid curve is a harmonic fit with annual, semiannual, and terannual components.

This year is chosen because it is near the middle of our data window analyzed and because the terannual component of the harmonic fit is well visible as relative increases around DOYs 100 and 250, respectively. Seasonal analyses for years 1987–2008 have been described by *Offermann et al.* [2010], and some long-term trends have been obtained.

[11] Here we analyze the temperature measurements from 1994 to 2009 for the fastest oscillations detectable by our technique. One infrared spectrum is taken every 1.3 min. As an example a data set resulting from 16 spectra in a 21 min interval is shown in Figure 2. Oscillation periods down to 2.6 min can be determined according to the Nyquist theorem.

[12] The data are analyzed on a nightly basis. Owing to the time resolution of our instrument the data are fairly noisy. This is partly due to the intensity fluctuations of the

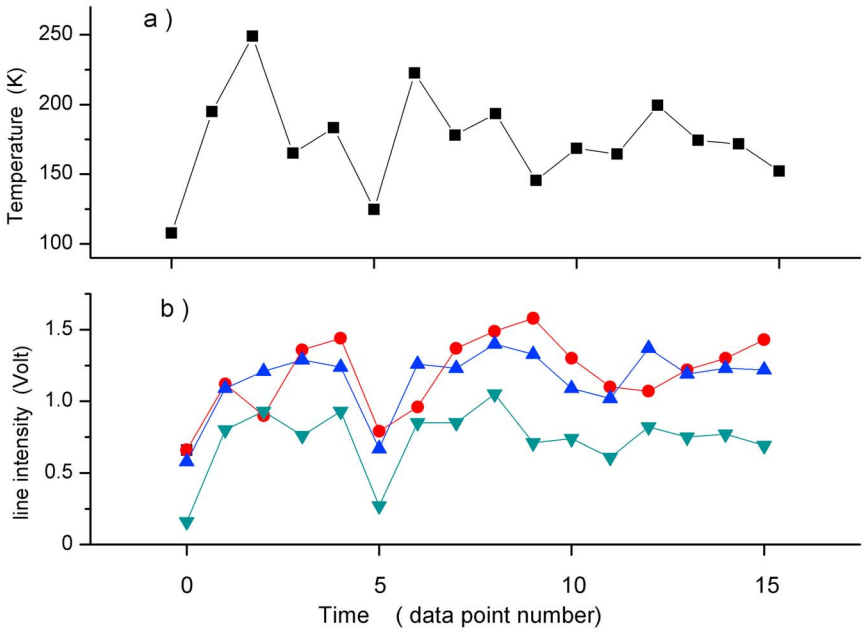

Figure 2. Data set of 21 min length. (a) Temperatures are derived from hydroxyl lines $P_1(2)$, $P_1(3)$, and $P_1(4)$ and (b) their intensities ($P_1(2)$, red; $P_1(3)$, blue; and $P_1(4)$, green). Time distance of data points is 1.3 min.

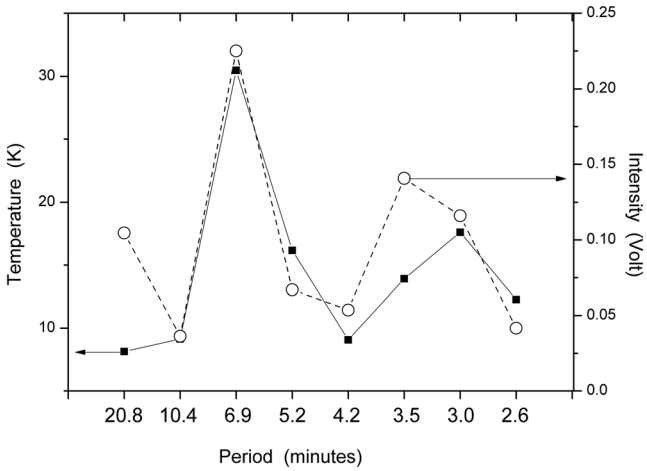

Figure 3. FFT spectra of the data shown in Figure 2. Temperature amplitudes are shown as squares (left ordinate), and mean intensity amplitudes are shown as circles (right ordinate) (see text).

three infrared lines used. Their noise is amplified by the nonlinear retrieval method used to determine the temperature [*Bittner et al.*, 2002]. As a measure of the temperature fluctuations we use the standard deviation σ_N from the nightly mean temperature. These σ_N values can be occasionally quite large (40 K). They contain both the noise and the atmospheric variations due to waves and "ripples" (see below).

[13] The objective of our analysis is to separate the waves from the noise. For this purpose we use a spectral analysis (FFT). As the noise can be much larger than the amplitudes of the atmospheric waves, it cannot be excluded that some noise fluctuations are mistaken as waves by the spectral analysis. To avoid a distortion of our results we use the following procedure: We perform an FFT analysis not only for the temperatures, but at the same time also for the intensities of all three infrared lines. A wave identified in the temperatures is accepted as valid only if it shows up in the intensities of the lines as well. An example is shown in Figure 2. For all subsequent analyses we use data sets of 16 data points, i.e., 16 measured intensity spectra for the FFT. The three FFT spectra of the three lines are averaged and compared to the temperature FFT spectrum. This is shown in Figure 3 for the temperature and intensity data of Figure 2. An FFT analysis of 16 data points yields amplitudes of eight spectral elements (21 min, 10.4 min, 6.9 min, 5.2 min, 4.2 min, 3.5 min, 3 min, and 2.6 min). We do not use the two end points of the spectrum. We count a wave event as valid only if (1) the temperature spectrum has a relative maximum at a given spectral position, i.e., the amplitude at this point is 5% larger than at its two neighbor positions, and (2) if the mean intensity spectrum has a corresponding maximum at the same spectral position. For the example given in Figure 3 this is the case at the period of 6.9 min. However, we also count an event as valid if the intensity maximum does not occur at the same spectral position as that of the temperature but at the neighbor position. In the example given in Figure 3 this occurs at 3 min and 3.5 min, respectively. The reason is the limited spectral resolution of our FFT. This may attribute a wave to a spectral position or to its neighbor if the wave period is about in the middle. Thus Figure 3 counts two maxima in total.

[14] Our analysis method is fairly conservative. It is justified as follows: If in the atmosphere there is a wave in the temperature this also causes a wave in the three intensity lines used by us. This is because temperature enters the equation of OH level excitation (exponentially). In general temperature variations and those of the intensities seen in the data may not be independent. There are three cases to consider: (1) If the mean of three intensity lines shows a wavelike structure and a temperature wave results (and vice versa) we count this as a valid event. (2) If there is an oscillation in the temperature but not in the intensities there are three possibilities: either the intensities have been disturbed too strongly (for instance by some noise) or the intensities have compensated to some extent, or there is no real wave in the temperature at all, i.e., it is accidental. In each of these cases the event/time interval considered is discarded as a candidate for containing a temperature wave. (3) There is an oscillation seen in the intensities, but not in temperature. This may for instance happen if the intensities are modulated in a wavelike form by some obstacle (cloud) in the field of view. In this case the three lines are changed by the same factor, and the retrieval algorithm does not yield a temperature change. Also this type of event is discarded.

[15] Our selection criterion thus is strict as quite a few (small) waves may be lost. It has, however, the advantage to exclude strong noise fluctuations in the temperature signal from being accidentally taken as real temperature waves. We have checked on this effect by dropping the requirement that an intensity maximum must be seen simultaneously with the temperature maximum. As expected the amplitudes given in Figure 4 below went up. The changes were moderate: between 10% and a factor 2.3.

[16] Our method thus yields lower limits for wave occurrence and wave amplitudes. It does not give a climatology as it is biased for instance toward high temperature

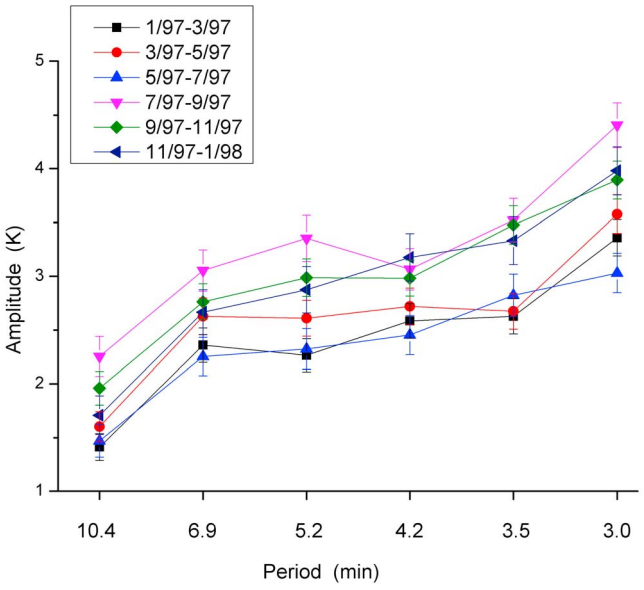

Figure 4. Mean temperature spectra in 3-monthly intervals in 1997.

amplitudes. This is, however, not a limitation for the present analysis as this studies relative variations, only.

[17] To obtain a general impression of the temperature spectra we have analyzed the data of all nights available in year 1997 which we use as a test year here. Again, data sets of 21 min length have been used. Amplitudes are very different and can be substantial (see Figure 3). We therefore calculate for a given oscillation period a mean amplitude per night which is weighted by the occurrence frequency. Resulting mean spectra are shown in Figure 4 for various times of the year 1997. The curves give means of three months each which are moved in steps of two months through the year (i.e., JFM, MAM, MJJ, JAS, SON, NDJ). The error bars are errors of the mean.

[18] The amplitudes are between 1 K and 5 K, which is typical also of other years. It is interesting to note an increase of amplitudes from long to short periods in Figure 4. This is essentially determined by the occurrence frequencies of the oscillation periods as the amplitudes are rather similar (±5%, decreasing from long to short periods). The increase is seen in a similar way in other years, too (1997–2009).

[19] Only part of the oscillations in Figure 4 can be gravity waves as these can exist only at periods longer than the Brunt-Väissällä period (5 min). Following suggestions by *Taylor and Hapgood* [1990], *Taylor et al.* [1997], *Hecht* [2004], and *Hecht et al.* [2007] we assume as a working hypothesis that our 3 min periods are "ripples" that are indicative of atmospheric instabilities. This is discussed in detail in section 6.1 below. The curves in Figure 4 indicate a seasonal variation of the amplitudes with greatest values in late summer and autumn. This will be discussed in detail below (section 4).

[20] We have checked whether the maximum criterion "5% larger than at its two neighbor positions" might be too weak. We have raised that value in steps up to 40%. This should decrease the mean amplitudes in Figure 4. It does as expected. The changes are, however, moderate. Up to a 20% criterion they are 7–25%. For the 40% criterion they are 50% to a factor 1.4. The relative form of the spectra remains about the same in all cases.

[21] We have also checked whether the increased maximum criteria affect the long-term correlation of the short-period proxy σ_a and the longer-period proxy σ_N discussed below (first and second paragraphs in section 4, and Figure 9). It is found that the long-term σ_a curve in Figure 9 is essentially unchanged in its relative structures. The correlation coefficients between σ_a and σ_N are slightly reduced by 4% in the 20% case and by 13% in the 40% case.

[22] It needs to be mentioned that the temperature changes shown in Figure 2a are very large, and high amplitudes result in Figure 3. This is not a common feature. These data rather were chosen to give a pronounced example. In general amplitudes larger than 25 K amount only to a few percent of occurrence for the periods shown in Figure 4. Temperature changes of 50 K or more within 1.3 min occur in less than 4% of the cases.

[23] The complexities of airglow wave structures in the upper mesosphere including line-of-sight cancellations have recently been demonstrated by *Snively et al.* [2010]. They show how difficult it is to analyze in detail spatial and temporal structures especially for measurements from a single station. We do not attempt this here but rather study the long-term stability or variation of our signatures.

3. Standard Deviations and Wave Amplitudes

[24] For a given time interval (e.g., one night) we calculate a mean temperature and the deviations from this mean. The corresponding standard deviation σ_N is a convenient parameter to estimate the magnitude of the temperature fluctuations in that time interval. These fluctuations contain contributions from genuine atmospheric noise, instrumental noise, gravity waves of various oscillation periods, and possibly other fast waves as tides and fast planetary waves. Figure 5 shows nightly standard deviations σ_N for the recent years in Wuppertal (black curve). The scatter of the σ_N data is fairly large and the data have therefore been smoothed by a 50-point Savitzky-Golay algorithm which has a good resolution [*Savitzky and Golay*, 1964]. This type of smoothing is used in all pictures given here if not stated differently. The error is estimated to ±0.7 K. The resulting values in Figure 5 are high and still quite variable. There are two major variations: a long-term change over several years, and a pronounced shorter variation during the course of the year which appears to recur in a similar manner each year. Either variation must have specific reasons beyond simple noise, because it is hard to believe that atmospheric and/or instrumental noise could have the time dependences shown. Especially interesting is the intra-annual variation which shows a pronounced peak in autumn and a smaller peak in spring. This pattern is seen in most of the years analyzed (see also Figure 9 below). To study whether this is a general structure or a feature specific to the Wuppertal measurement site, we have added a second data set to Figure 5 (red curve). It shows σ_N values measured by our twin instrument GRIPS I at Hohenpeissenberg. Note that this curve has been shifted upwards by 10 K to better distinguish it from the Wuppertal curve. The σ_N values at the two places are fairly similar, those at Hohenpeissenberg being somewhat larger. The intra-annual variations with the two peaks mentioned are found at Hohenpeissenberg, too. Hence, these features are general structures, indeed.

[25] Gravity wave activity is believed to influence the mesosphere and its circulation [e.g., *Holton*, 1983; *Jiang et al.*, 2006]. This should somehow be linked to our σ_N values. As gravity waves can have periods and wavelengths of very different magnitudes it needs to be determined which wave has which effect? We start here with the shortest periods we can measure as described in section 2. Afterwards we compare them with σ_N which covers somewhat longer periods.

[26] As mentioned before, we use the year 1997 as a test year. To express the amplitudes of the short periods in terms of standard deviations we calculate an equivalent standard deviation σ_a for the shortest oscillations. For this we calculate for each period i (i = 1–6) given in Figure 3 the mean amplitude $\bar{a}_i$ in a given night. Only nights with more than five data sets of 21 min available are considered. Parameter σ_a is then calculated from equation (1).

$$\sigma_a = \sqrt{\frac{1}{2}\sum_{i=1}^{6} \bar{a}_i^2} \tag{1}$$

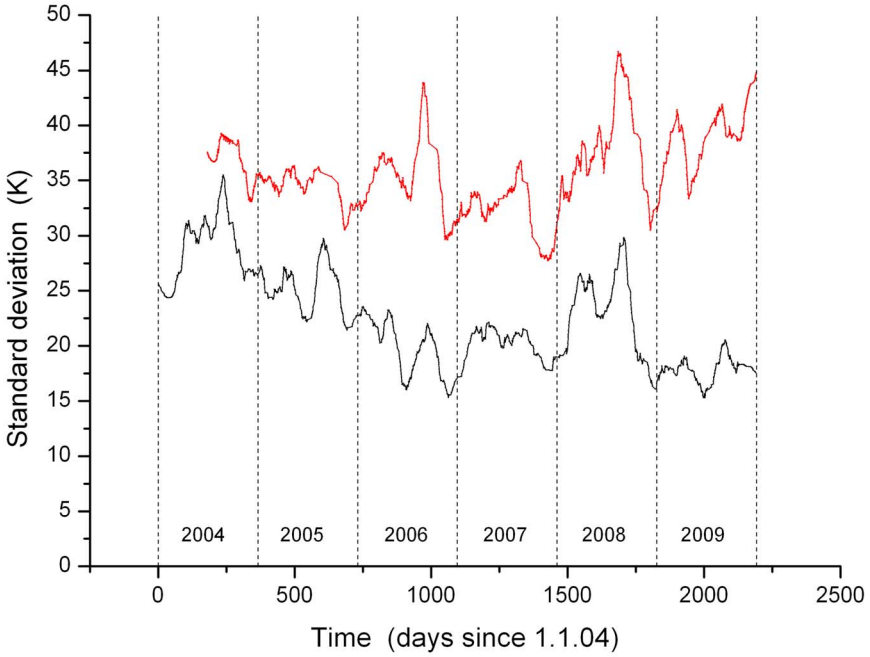

Figure 5. Nightly standard deviations σ_N from mean temperatures during the course of years 2004–2009. Data have been smoothed by a 50-point Savitzky-Golay algorithm. Black curve shows results from Wuppertal (51°N, 7°E, GRIPS II), and red curve shows those from Hohenpeissenberg (48°N, 11°E, GRIPS I). The red curve has been shifted upward by 10 K for clarity.

The resulting σ_a values are used as a measure of short-period wave/oscillation activity. These values are plotted for all nights in 1997 versus σ_N in Figure 6. A close correlation is obtained with a correlation coefficient r = 0.91. The slope of the regression line is 0.38 K/K. If the whole smoothed data set 1994–2009 discussed below is used, the respective numbers are r = 0.94 and slope = 0.40 K/K.

[27] The time dependence of σ_N and σ_a during the course of the year 1997 is shown in Figure 7. As shown by the slope of the line in Figure 6 σ_a amounts to about 40% of σ_N. A 20-point smoothing has been applied for the two curves. The two curves are nearly parallel, i.e., their relative variations are very similar. This indicates that the regression line

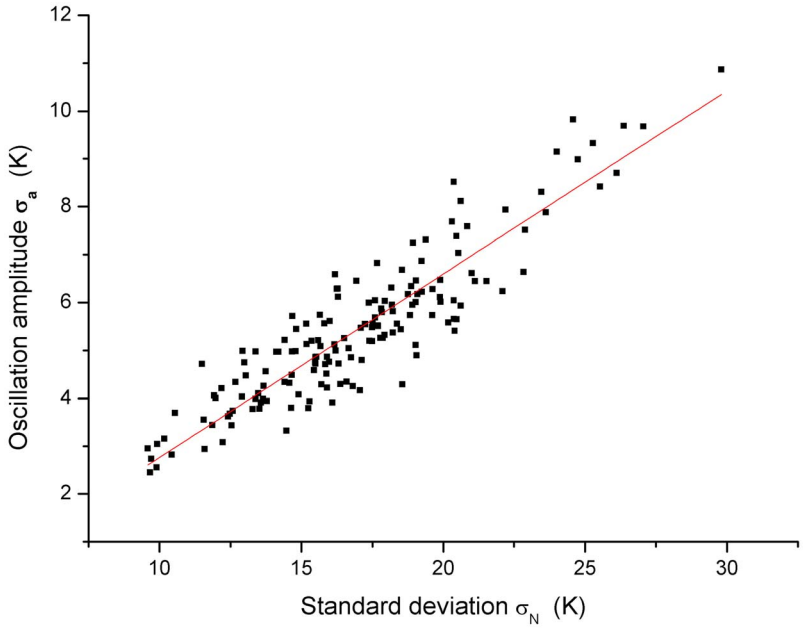

Figure 6. Short-period oscillation amplitudes σ_a compared to temperature standard deviations σ_N in 1997. Correlation coefficient is r = 0.91. Slope of regression line is (0.38 ± 0.012) K/K (see text).

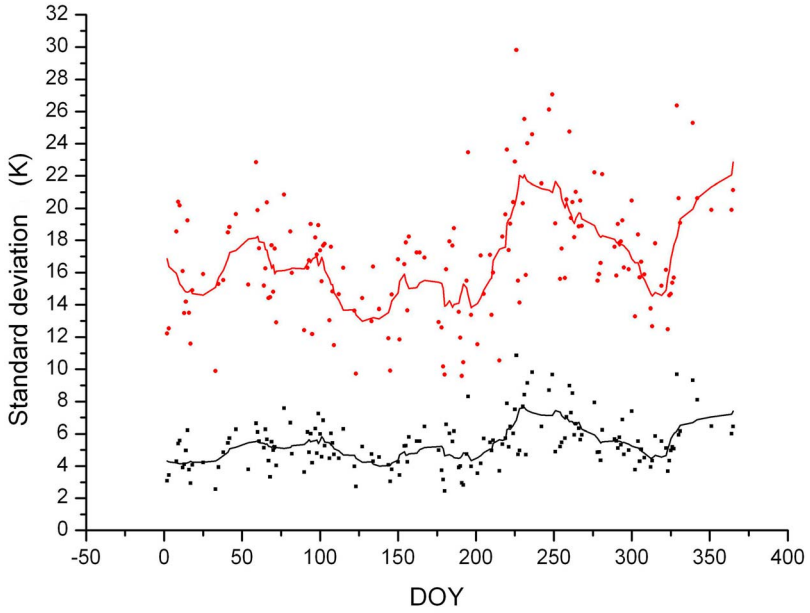

Figure 7. Time development of parameters σ_N (red) and σ_a (black) of Figure 6 during 1997. Solid curves show a 20-point smoothing.

in Figure 6 is representative of all parts of the year. The errors are about ±0.3 K for σ_a and ±0.7 K for σ_N.

[28] The parameter σ_a is a cumulative measure of the amplitudes of the six oscillation periods. It remains to be determined whether or not the amplitudes of the individual periods also behave similarly, or whether certain periods might show a peculiar behavior. This might happen because the shortest periods (3–4.2 min) may be of other origin than the longer periods (6.9–10.4 min) (ripples versus gravity waves, see section 6.1, 6.2). To check on this we plotted the amplitudes of the six periods similarly as in Figure 7 and smoothed them accordingly. These mean curves are shown in Figure 8 together with those of σ_a and σ_N as references. The estimated errors are ±0.7 K for σ_N, and between ±0.25 K and ±0.35 K for the other curves. The curves are quite similar and follow more or less the main features of σ_a and σ_N with their flat maximum in spring and a more pronounced maximum in late summer. Figure 8 shows that σ_a and also σ_N is a reasonable representation of the oscillation activity at these short periods.

[29] These results demonstrate a significant contribution of the very short period wavelike structures to the nightly data variance. About 40% of σ_N can be ascribed to them. The remaining variance must be due to other longer-period gravity waves, noise, etc. The importance of the short oscillations is further discussed in section 6.

4. Seasonal Variations

[30] Temperature standard deviations σ_N as shown in Figure 5 are available at Wuppertal back to 1994. This 16 year data record is shown in Figure 9. A 50-point smoothing has been used. Errors are as in Figure 5. The modulation structure with one or two peaks per year is seen in almost all of the years. Superimposed is a long-term increase 1994–2004 with an apparent trend break around 2004, and a decrease in the following years. The whole data set 1994–2009 shows a positive trend of (0.29 ± 0.02) K/a (dashed line in Figure 9). The size of the seasonal peaks is very variable (see also Figure 5).

[31] We have added in Figure 9 the long-term developments of σ_a (blue) and of the amplitudes of our shortest oscillation (3 min, red). This is because we want to check again on possible differences between the shortest oscillation (3 min) taken as an indication of ripples and the other oscillations contained in σ_a (see Sections 6.1, 6.2). The attribution of the 3 min period to ripples is discussed in Section 6.1 below. The errors of the two curves are ±0.2 K and ±0.25 K, respectively. There are several data gaps in these curves. They mostly occur because only nights with more than five data sets have been used for improved statistics. The curves follow the major structures of σ_N quite well. The correlation of σ_N with σ_a has a coefficient r = 0.94. The slope of the regression line is 0.40. The correlation coefficient of the 3 min amplitudes with σ_N is r = 0.88 (slope is 0.26). That of the 3 min amplitudes with σ_a is r = 0.94 (slope is 0.66). This close relationship of the three parameters is interesting and allows using one (σ_N) for the others. (If unsmoothed data are correlated the coefficients are between 0.57 and 0.88.) A trend of (0.12 ± 0.01) K/a is obtained by fitting a linear regression to the σ_a data (not shown in Figure 9). The corresponding numbers for the 3 min oscillation are (0.061 ± 0.008) K/a. The σ_N data series of Hohenpeißenberg (Figure 5) appears to show a trend different from that at Wuppertal. This series is, however, too short to draw significant conclusions.

[32] In an attempt to understand the nature and variability of the seasonal peaks of σ_N we have calculated a seasonal mean, i.e., the average of all years shown in Figure 9. The result is given in Figure 10. The data are again very variable and have therefore been smoothed by a 50-point running mean (red curve; the error is about three times the thickness

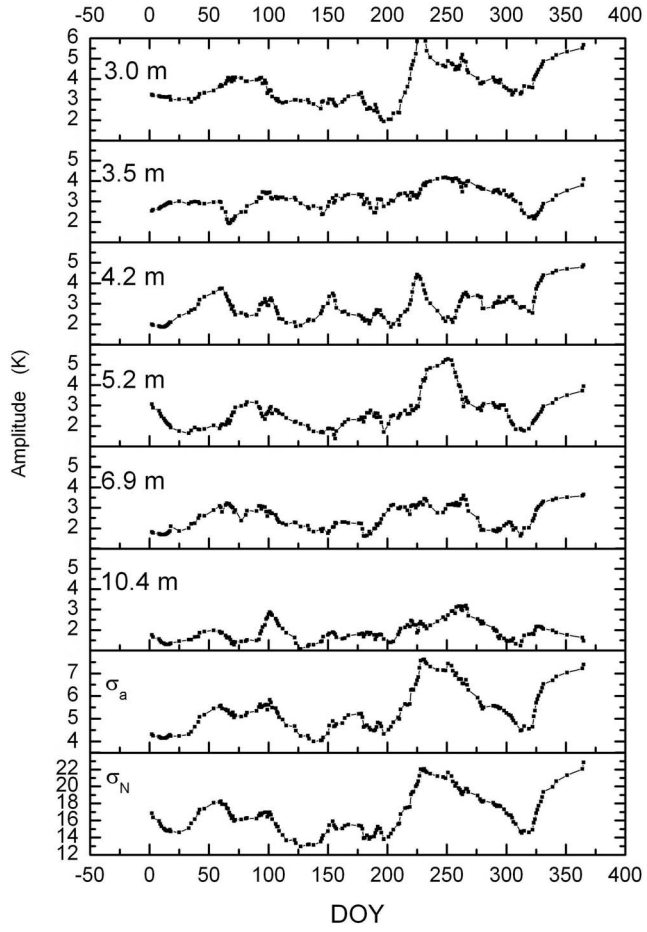

Figure 8. Amplitudes (K) of six oscillation periods given in Figure 3 during 1997. Parameters σ_a and σ_N from Figure 7 are shown for comparison. A 20-point smoothing has been applied. Periods 3.0 m, 3.5 m, and 4.2 m are believed to be "ripples," and longer periods could be "ripples" or gravity waves (see text).

of the line). This mean curve exhibits a seasonal structure as expected from the single years. There is a pronounced late summer peak around DOY 237 and a smaller and broader peak in spring around DOY 108.

[33] We have compared this to the turnaround times (times of zonal wind reversal) in the middle stratosphere (20 hPa altitude). The autumn reversal is at about DOY 244. The spring reversal shows a trend from DOY 110 to DOY 130 between 1988 and 2008. These times are indicated in Figure 10 by vertical dashed (black) lines and by a horizontal black arrow. These times are taken from *Offermann et al.* [2010, Figure 13]. Zonal wind reversal at the altitude of the OH measurements is of greater interest, but cannot be so easily determined. Radar wind measurements nearest to Wuppertal are taken at Juliusruh (55°N, 13°E). They are available at 94 km altitude [*Offermann et al.*, 2010, Figure 15] and show a spring reversal with a trend from DOY 148 to DOY 136 in the time interval 1993–2008. This is indicated by red dashed vertical lines and a red horizontal arrow in Figure 10. The mean value of the autumn turnaround of the radar winds near the mesopause is difficult to determine [*Offermann et al.*, 2010]. We therefore use corresponding radar data at somewhat lower altitude (80 km) from *Keuer et al.* [2007]. They find the autumn reversal near DOY 255 (red vertical dashed line in Figure 10) with a small tendency to shift toward later times.

[34] We thus find that the maxima of the temperature standard deviation σ_N occur before the circulation reversal in the stratosphere (at 20 hPa) as well in spring as in autumn. This applies even stronger to the mesosphere near the OH altitude. It should be noted that in the upper mesosphere the time of turnaround does not change much with altitude.

[35] It is widely believed that gravity waves propagating upwards in the middle atmosphere tend to break and produce turbulence in the 80–90 km altitude regime. This can be seen, for instance, in the recent WACCM 3.5 whole atmosphere model. This model uses a parameterization of both orographic and nonorographic GW. Details of the parameterization are described by *Garcia et al.* [2007]. The parameterization of nonorographic waves now includes variable GW sources that depend on frontal systems and convection calculated in the model [*Richter et al.*, 2010]. In the upper mesosphere parameterized GW dissipation leads to eddy diffusion of potential temperature and constituents which can be represented as vertical diffusion with coefficient K_{zz} (see *Garcia et al.* [2007, Appendix A4] for a description of the formulation). Figure 11 shows monthly mean K_{zz} averaged over a four-member ensemble of WACCM simulations over the period 1987 to 2005. These simulations were conducted as part of the Stratospheric Processes and their Relation to Climate 2nd Chemistry-Climate Model Validation (SPARC CCMVal-2) activity [*Eyring et al.*, 2010; *Morgenstern et al.*, 2010].

[36] The data in Figure 11 are from 19 years of free model runs for an altitude of 85 km. Results at 90 km and 95 km altitude look essentially the same, however, the values are somewhat larger. The eddy coefficients show a pronounced seasonal variation with a high peak in autumn and a slightly broader and smaller peak in spring. This structure is similar to that seen in the temperature standard deviations in Figure 10. The eddy peak values in April, May, and September in Figure 11 (DOYs 105, 135, and 258) are given in Figure 10 as vertical dash-dotted green lines. They occur near to the turnaround times and hence near to the σ_N maxima.

[37] In Figure 11 we have added for comparison the turbopause altitudes as derived by *Offermann et al.* [2007] (errors are a few km and are given in detail in their Figure 6). At a fixed observation height (e.g., 90 km) one would expect high gravity wave amplitudes if the turbopause is at low altitude, and vice versa. We have therefore reversed the scale in Figure 11 for better comparison with K_{zz}. A close correspondence of the two curves is seen. It suggests that around months 4, 5, and 9 there is considerable gravity wave activity leading to strong turbulence production.

[38] We have also compared the monthly eddy values in Figure 11 with monthly mean σ_N values computed from Figure 10. Again, the two curves are quite similar. The correlation coefficient is 0.71 at 99% significance. The similarity is important as data from a global model (WACCM) are compared here to measurements taken at a local station (Wuppertal). These results together with those of Figures 6–9 suggest that our σ_N parameter is related to gravity wave activity as well as gravity wave breaking, and

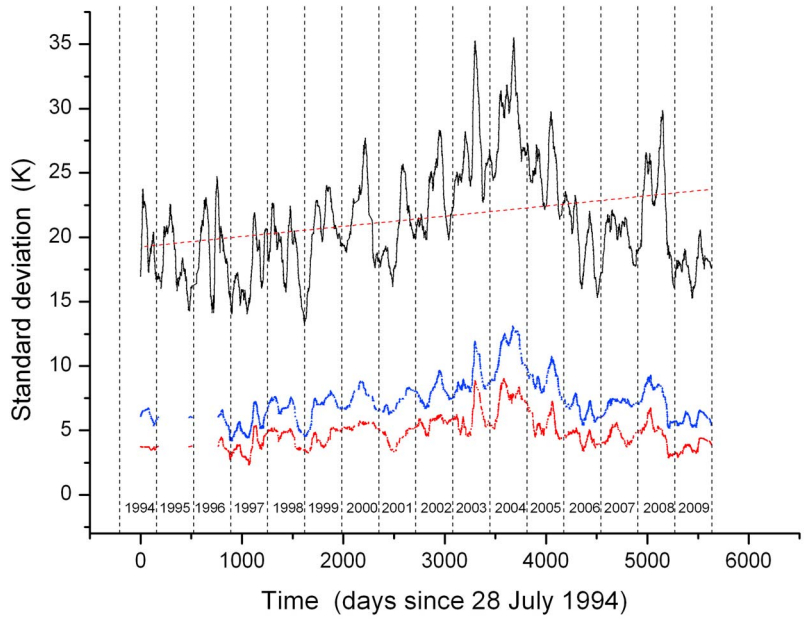

Figure 9. Temperature standard deviations (black) as in Figure 5, but for the extended time interval 1994–2009 at Wuppertal. For comparison, σ_a (blue) and 3 min amplitudes (red) are given (see text). A 50-point smoothing has been applied.

we will therefore tentatively use it as a corresponding proxy in the following. It should be mentioned that the very short period structures (ripples) are also expected to collapse into turbulence [e.g., *Hecht et al.*, 2007].

[39] It is interesting to note that there is a similar correspondence of our K_{zz} and σ values derived from SABER data [*Offermann et al.*, 2009, Figure 8] at lower altitudes (70–80 km). There is, however, only one seasonal K_{zz} maximum at these altitudes. It occurs in summer (July) and

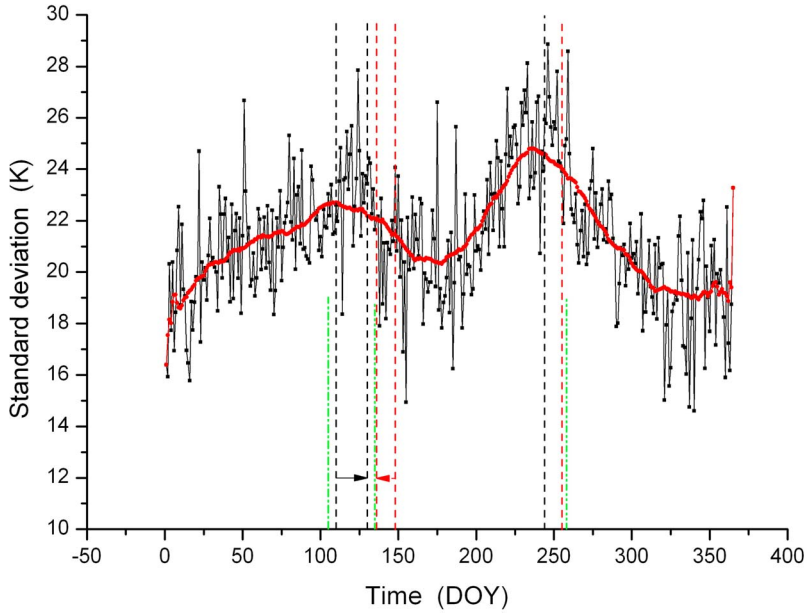

Figure 10. Mean temperature standard deviations σ_N for the years given in Figure 9 (1994–2009). The seasonal variation is shown by the red curve (50-point running mean). Vertical dashed lines indicate circulation turnaround in the stratosphere (black) and mesosphere (red). Black arrow indicates a trend in the stratosphere in the time interval 1988–2008. Red arrow indicates a trend in the mesosphere in the time interval 1993–2008. Green dash-dotted vertical lines indicate the maxima of eddy coefficients in Figure 11. For details see text.

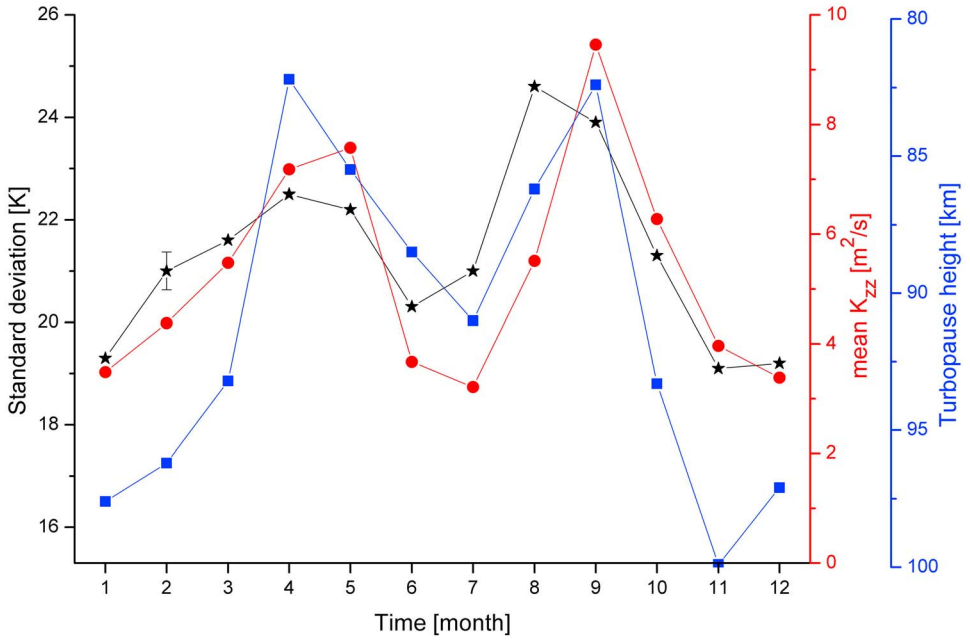

Figure 11. Turbulent eddy coefficients K_{zz} (red dots) as derived by the WACCM 3.5 model. Nineteen years of free model runs have been averaged, and resulting monthly means are shown for 85 km altitude. The turbopause height [*Offermann et al.*, 2007] is given for comparison (blue squares). Please note that its ordinate has been inverted (see text). Temperature standard deviations σ_N (black stars, left ordinate) are monthly means from 1994 to 2009 (87 km altitude). The error bar shown for February is the error of the mean and is typical of the other months.

meets a corresponding maximum in the SABER data, indeed. This shows that the seasonal structures are very variable with altitude which is discussed below (section 6.3).

5. Intradecadal and Interdecadal Variations

[40] In addition to the pronounced seasonal variations of the temperature standard deviations σ_N there are substantial long-term changes as shown by Figure 9. There is a decadal increase until 2003/2004 and a subsequent decrease toward 2009. In addition, there appear to be intradecadal variations superimposed. To separate these variations from the seasonal variations and to show the structures more clearly Figure 12 presents yearly mean values of σ_N. These are calculated from 1 January to 31 December and are plotted in the middle of the year in Figure 12. In order to increase the time resolution of this analysis we have shifted the data series by half a year and calculated corresponding yearly means from 1 July to 30 June of the next year.. These are plotted at the end of the year in Figure 12. For comparison Figure 12 shows corresponding annual amplitudes A_1 of the harmonic analyses described above (red curve).The error of σ_N is about double the size of the symbols. The error of A_1 is ±1.6 K according to *Offermann et al.* [2010, Figure 4].

[41] The increasing or decreasing trends of σ_N before and after 2004 are shown in Figure 12 by linear regression lines. Fit intervals are 1 July 1994 to 1 January 2004, and 1 January 2004 to 1 January 2009, respectively. The differences of the measured data points and the fit lines (residues) show values of several Kelvin and thus are relatively large.

[42] A linear fit line has also been drawn to the A_1 data in Figure 12 (1994–2009), and substantial residues are seen here, too. A weak trend break at 2004 is found in the A_1 data as well. It is, however, so weak that it is disregarded here.

[43] It is very interesting to note that the two types of residues in Figure 12 are in antiphase with each other, i.e., a positive residue in σ_N corresponds to a negative one in A_1, and vice versa. We have calculated the correlation coefficient to be r = −0.63 with a significance of 99%. The slope of the corresponding regression line is −0.47 K/K.

[44] If a fit is calculated for the whole σ_N data set in Figure 12 its slope is (0.32 ± 0.13) K/a. The slope of the corresponding A_1 fit line is −0.042 K/a. The correlation of these data is marginal with a correlation coefficient of −0.38. The gradient of the regression line is –0.17 K/K. It has the same sign as the corresponding value of the residues but is quite a bit smaller.

[45] We have increased the time resolution of the analysis of the whole σ_N data set by calculating trends on a monthly basis instead of an annual basis. The results are shown in Figure 13. The monthly trends are near the slope of the entire data set of 0.32 K/yr. They are, however, not constant during the year but show seasonal variations with a broad maximum in late summer/autumn and another one in spring/early summer (see the hatched areas in Figure 13; the horizontal bar from February to November is meant to guide the eye). There are pronounced minima in February and November. These structures are not too conclusive considering the error bars. Nevertheless, the two broad maxima may be interpreted as time periods of increasing gravity wave activity and hence of dynamical forcing, if we assume

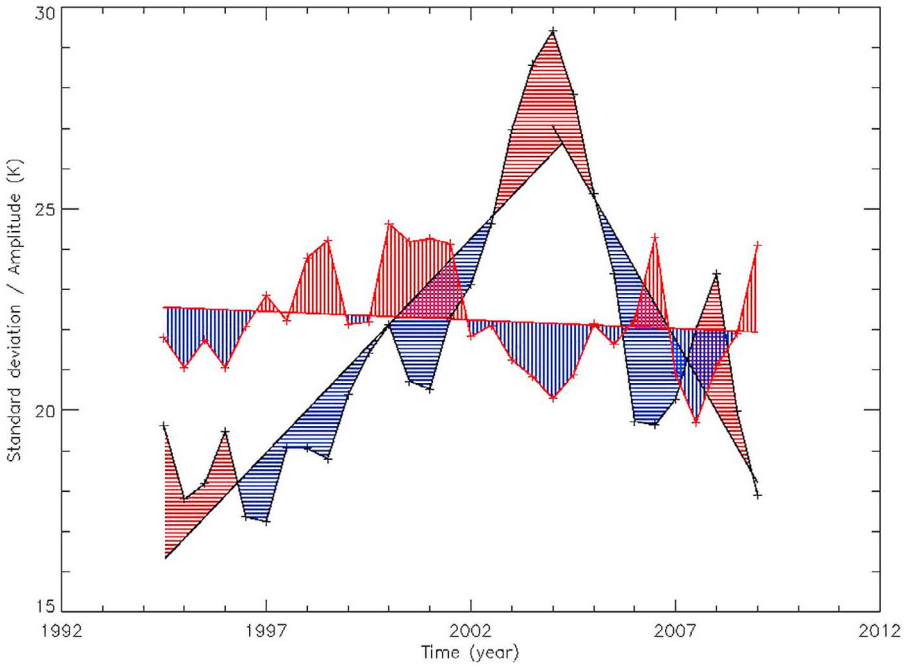

Figure 12. Comparison of yearly mean temperature standard deviations σ_N (black lines and pluses) and harmonic annual fit amplitudes A_1 (red lines and pluses). Data series have been shifted in addition by one half year for increased time resolution (see text). Straight lines are least square fits. Deviations from the fit lines (residues) are shaded red (blue) if positive (negative). Red and blue areas of the two parameters are anticorrelated (see text).

our standard deviations σ_N as proxies for wave breaking. The seasonal structure is similar to the general GW structure seen in Figure 10. To indicate this, the mesosphere turnaround times shown in Figure 10 are also shown in Figure 13 as red dashed vertical lines. It is apparent that the two maxima in Figure 13 occur at the same times or somewhat earlier than those in Figure 10. Hence, if our σ_N is indicative of GW breaking a large and increasing part of it occurs before turnaround.

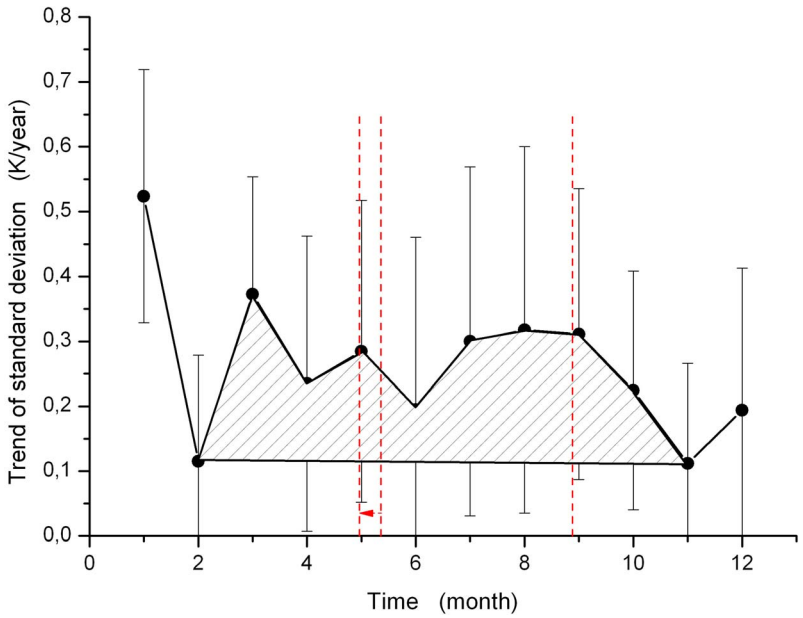

Figure 13. Long-term increase (trend) of temperature standard deviations σ_N on a monthly basis. Trend interval is 1994–2009. Vertical dashed red lines indicate circulation turnaround in the mesosphere and are taken from Figure 10. Red arrow indicates a shift in the time interval 1993–2008.

[46] We have checked whether the long-term trends would influence the seasonal variation of σ_N (Figure 10). Therefore we divided our data set in two subsets: 1994 to 2001 and 2002 to 2009, respectively. Corresponding seasonal variations were determined as in Figure 10 (not shown here). The curve of the later time interval is a few K above that of the earlier interval because of the trend increase in nine years. Otherwise the seasonal variation has not much changed in this time span. This was to be expected from Figure 13.

6. Discussion

6.1. Short-Period Spectra

[47] Waves with short periods and short horizontal wavelengths have been intensively studied in the recent years by various types of airglow imagers [e.g., *Hecht*, 2004; *Hecht et al.*, 2005, 2007; *Taylor et al.*, 2007; *Medeiros et al.*, 2007; *Nielsen et al.*, 2009; *Simkhada et al.*, 2009, and references therein]. Major wavelike structures observed are "bands" and "ripples." Band structures are larger than ripples, with horizontal scales on the order of 25 km versus 15 km [*Hecht*, 2004]. Time periods are on the order of 4–40 min for bands and 3–10 min for ripples. Even shorter periods down to below 1 min) have been occasionally reported as ripples [*Hecht*, 2004].

[48] The band structures are widely believed to show fast gravity waves traveling from the lower atmosphere to the mesopause and eventually breaking there. Vertical wavelengths are on the order of 35 km, i.e., much larger than the OH layer thickness [*Li et al.*, 2005].

[49] Ripples are thought to originate in situ from local nonlinear interactions of wind shears with gravity waves leading to Kelvin-Helmholtz instabilities, and from convective instabilities [*Taylor and Hapgood*, 1990; *Horinouchi et al.*, 2002; *Hecht*, 2004; *Li et al.*, 2005, *Hecht et al.*, 2005, 2007; *Fritts et al.*, 2009]. They are thus indicative of dissipating gravity waves. If these structures move or are transported with the wind through the field of view of an upward looking OH instrument like GRIPS they could have a wave-like appearance [e.g., *Hecht et al.*, 2007]. The apparent oscillation period would be influenced by the wind speed.

[50] In our spectra (Figures 3 and 4) with periods ranging from 3 to 10 min we could see short-period gravity waves as well as ripples. We cannot distinguish between them as imager measurements can do [e.g., *Taylor et al.*, 1997]. However, amplitudes at periods shorter than the Brunt-Väissällä frequency (5 min) can hardly be gravity waves (if we neglect Doppler shifting and evanescent waves [e.g., *Hecht et al.*, 1995, 2007; *Yue et al.*, 2010]). It needs to be mentioned that the period limitation to greater than 5 min is valid for the intrinsic frequencies. *Nielsen et al.* [2009] have shown, however, that the average distributions of observed and intrinsic periods of gravity waves are rather similar. This leads us to use apparent (observed) periods here.

[51] Many histograms of the occurrence of band and ripple periods have been published [e.g., *Taylor et al.*, 1997; *Nakamura et al.*, 1999, 2003; *Pautet et al.*, 2005; *Medeiros et al.*, 2007; *Suzuki et al.*, 2009]. Imagers find the shortest ripple periods to be well below shortest gravity wave (band) periods. Shortest ripple periods are found down to below 2.7 min by *Taylor et al.* [1997] and down to below 1 min by *Hecht* [2004]. In a detailed analysis of measurements with enhanced spatial resolution *Hecht et al.* [2007] identify the vast majority of features with periods below 4 min as ripples. They find wavelike structures down to periods below 2 min. The maximum of counted numbers of these ripples is found around periods of 3 min. These are observed periods that can be directly compared to our results (Figures 3 and 4). The increase of our amplitudes toward shorter periods in Figure 4 compares favorably with the results of *Hecht et al.* [2007, Figure 7]. It should be noted that *Hecht et al.* [2007] analyze intensity structures, only, whereas our oscillations are seen in temperature as well as in intensity.

[52] On the basis of the work cited we assume here as a working hypothesis that our oscillations at periods of 3 min are ripples. Our parameter σ_a is a superposition of gravity wave and ripple activity. We thus tentatively use our 3 min amplitudes as indication (proxy) of unstable (dissipating) gravity waves or atmospheric instability events involving gravity waves. The following analysis will show how far this assumption carries. The high correlation of the 3 min amplitudes with parameter σ_a obtained above (section 4) shows that σ_a is indicative of unstable gravity waves, too.

[53] Ripples are expected to mostly decay into turbulence [e.g., *Hecht et al.*, 2007]. The above shown high correlations of our 3 min amplitudes with our gravity wave proxy σ_N on the one hand, and of σ_N with the eddy coefficients K_{zz} on the other are in line with this expectation.

[54] Not much seems to be known about power spectra at these short periods because emphasis in the literature is mostly on structures with periods longer than the Brunt-Väissällä period [e.g., *Dewan et al.*, 1992; *Hecht et al.*, 2007]. It should be noted that our spectra (Figure 4) cannot be compared to standard power spectra directly because our analysis method emphasizes strong oscillations and we show weighted amplitudes.

6.2. Standard Deviations as Wave Proxies

[55] Our parameter σ_N is the temperature standard deviation in one night. It is used here as a proxy for gravity waves as has been done in many publications since the early work of *Fetzer and Gille* [1994] and *Wu and Waters* [1996]. In Figure 6 we demonstrate a very close correlation of the two parameters σ_a and σ_N, and in section 4 we find the same for the 3 min amplitudes and σ_N. If the 3 min amplitudes and σ_a are proxies for breaking gravity waves, this correlation means that some part of the gravity waves present in σ_N are unstable. This is not unreasonable at the altitude of 87 km as gravity waves are generally assumed to break in the 80–90 km regime. It is in line with Figure 11 which shows a close correlation of σ_N and the eddy coefficients K_{zz} at 85 km, as mentioned.

[56] The parameter σ_N is very useful to analyze various wave features in an easy way. It needs to be noticed, however, that it takes into account only short- and medium-period waves as it is restricted to the nightly measurement time of a few hours. The parameter σ_a is also highly selective (e.g., concerning the wavelength). It selects waves/oscillations that are visible in temperature and transport (i.e., intensity) simultaneously. One could thus suspect that the very short oscillations (3–10 min) might not be typical of the atmosphere. Figure 8 shows, however, that the seasonal

variations (in 1997) of the shortest periods, of σ_a, and of σ_N are quite similar. The correlation of the 3 min data with σ_N in Figure 8 yields, for instance, a coefficient r = 0.59. The slope of the regression line is 0.29 K/K. The corresponding numbers for the larger data set in Figure 9 are r = 0.88 and 0.26 K/K, respectively. This confirms the connection of ripples and general gravity waves if it is assumed that the 3 min data represent the former, and σ_N the latter.

[57] The slope of the regression line σ_a versus σ_N is 0.38 K/K in Figure 6 and 0.40 K/K in Figure 9. Hence, σ_N contains a substantial amount of fluctuations beyond the very short oscillations shown in Figure 4. These may be longer-period gravity waves. They could, however, also be some short-period features that were neglected because our analysis method yields lower limits, only.

6.3. Seasonal Variations

[58] Seasonal variations of gravity wave activity are interesting because the corresponding wave breaking is thought to control the large scale circulation in the mesosphere [*Holton*, 1983]. Gravity wave maxima in summer and in winter are believed to explain zonal wind turnaround in spring and autumn. Corresponding seasonal variations have been inferred by various model studies [see, e.g., *Fritts and Alexander*, 2003].

[59] Many wind measurements by ground based radars have been performed, and frequently found the above mentioned semiannual variation with gravity wave maxima at solstices, sometimes superimposed on an additional annual variation [e.g., *Manson et al.*, 1999; *Beldon and Mitchell*, 2009; *Placke et al.*, 2010, 2011, and references therein]. Details of this basic picture can be quite different at least at times as gravity waves are found to be strongly dependent on parameters like altitude, latitude, local station, and their period and wavelength. *Dowdy et al.* [2007] found a mixture of annual and semiannual variations that was different at 80 km and 90 km, depending on the wave periods. The relative share even reversed from the lower to the higher altitude. A peculiar altitude dependence was also seen by *Jacobi et al.* [2006], with an annual variation at lower altitudes, i.e., a summer solstice maximum that split and moved toward the equinoxes at the higher altitudes. It is interesting to note that annual and/or semiannual variations are frequent in mesospheric and lower thermospheric airglow intensity, and a similar transition from an annual variation at lower altitudes to a semiannual variation at higher altitudes was reported by *Liu et al.* [2008]. Much interannual variation of the seasonal gravity wave changes is also seen.

[60] Seasonal satellite measurements have also been reported by *Jiang et al.* [2006]. They analyzed MLS data measured on the AURA satellite at high latitudes (and 80 km altitude) and found a semiannual oscillation with maxima near solstices in the mesosphere and an annual variation in the upper stratosphere.

[61] The seasonal curves presented here (Figures 5 and 7–11) are different. The characteristic seasonal structure is a double peak with one maximum near spring turnaround and another one near autumn turnaround (Figure 10). However, it does not occur in every year. Sometimes the two peaks seem to be merged into one (summer) peak (Figure 9). Another difference is that at the end of most years there is a deep minimum and not a winter maximum as reported in much of the literature.

[62] Temperature measurements from SABER on the TIMED satellite have been analyzed by *Preusse et al.* [2009] and *Offermann et al.* [2009]. The latter authors find a double peak structure in the summer half of the year with maxima in April/May and July/August, respectively (at 50°N, Offermann et al.'s Figure 8). This is very similar to the double structure shown here in April and August (in Figures 10 and 11). An even better agreement is obtained between the mean curve in time interval 2002–2009 (see above Section 5, last paragraph) and Figure 6 of *Offermann et al.* [2009] (2002–2005, 88 km) which gives a closer comparison in altitude and time interval. The correlation coefficient of these two curves is 0.53 at 93% significance).

[63] The double peak structure is seen by *Offermann et al.* [2009] not only at 50°N and 88–90 km, but appears to be present in a similar form also at 70°N (90 km and 100 km, Offermann et al.'s Figure 8). It is important to note that at 50°N and different altitudes (10 km lower and higher than 90 km) the seasonal variations look fairly different (maxima near summer and winter solstices). The same applies to 70°N at lower altitudes (winter maxima only). Hence, the seasonal variation of gravity waves is quite variable with altitude and latitude. This may explain the variety of results reported in the literature.

[64] Another reason of the different experimental results may be the differences in measurement techniques. Radar wind data yield kinetic energies of gravity waves whereas OH temperature data yield potential energies. These different energies have sensitivity to different gravity wave frequencies as was shown by *Geller and Gong* [2010]. Different frequencies, however, may have different seasonal variations [e.g., *Dowdy et al.*, 2007]. Gravity wave results recently published by *Yang et al.* [2010] appear to fit this picture. They derived gravity wave activity from temperature perturbations and showed semiannual maxima near the equinoxes.(These lidar measurements were taken at 23°S.)

[65] Our gravity wave proxy σ_N is correlated with wave breaking and turbulence production. The close correspondence of σ_N (16 years of local OH temperature measurements), eddy coefficients (global GCM, 19 years), and the turbopause height (4 years of SABER data, Figure 11) yields a consistent picture even though the data sets are rather different. The physical relation between our two seasonal gravity wave maxima and the circulation turnaround times needs to be determined yet.

6.4. Decadal Variations and Trends

[66] Long-term variations of mesospheric winds and other parameters have frequently been discussed in the literature. This includes trend-like developments as well as frequent trend breaks [e.g., *Portnyagin et al.*, 2006; *Laštovička et al.*, 2008, 2010; *Laštovička*, 2009, and references therein]. Little seems to be known about long-term changes of gravity wave activity. *Jacobi et al.* [2006] report on solar cycle dependence of this activity (see also the references therein). No conclusive results appear to be available for longer-term trends. Considering the consequences of gravity waves for mesospheric energy and momentum budgets, a search for a trend appears to be important.

[67] Our long-term data are shown in Figure 9. Here, solar cycle influences, if present, should show up with the maximum around years 2000/2001 and the solar minima around 1996 and 2008/9. Variability of the data is high, however, and in consequence a solar cycle signature cannot be identified. A substantial long-term trend is seen, though, with a break in 2004 (Figure 12). If the data are fitted without a break the trend is still there, but much weaker (Figure 9).

[68] We interpret this trend as an increasing gravity wave activity with associated dissipation. If this is true there should be a corresponding change of mesospheric circulation. This is found, indeed, in the data of *Keuer et al.* [2007]. These authors analyzed radar wind measurements at Juliusruh (55°N, 13°E) and found a long-term increase of the zonal wind speed U in summer in the time frame 1993–2005 at altitudes 85 km and 90 km (Keuer et al.'s Figure 15). The mean trend at the two altitudes is (0.52 ± 0.03) m/s per year. It is a mean value for the whole summer from April to September. This compares to an increase of the gravity wave proxy σ_N of 0.32 K/year. We call the ratio of the two numbers a trend sensitivity S_t which then results to S_t = 1.6 (m/s)/K.

[69] Superimposed on the fit lines of *Keuer et al.* [2007] are several intradecadal fluctuations (residues with respect to the fit lines). The most pronounced ones are in the years 2001–2002 for low values of U and 2003–2005 for high values. The mean swing between these two intervals is 7.5 m/s. There are corresponding fluctuations (low/high) of our σ_N in the same time intervals, with a swing of 3.4 K (Figure 12). The resulting sensitivity of the residues is S_r = 2.2 (m/s)/K. Hence the two sensitivity values are close together and are essentially the same if the errors (±49%) are taken into account. We conclude that the intradecadal influence of the gravity waves on the circulation (U) is about the same as for the extradecadal trends with a mean sensitivity of S = 1.9 (m/s)/K. It should be noted that we compare here annual σ_N values with zonal winds in summer. This is, however, not a strong limitation because the winter winds have almost no trend.

[70] The seasonal temperature variation in the upper mesosphere (Figure 1) is closely linked to the atmospheric circulation. If there is a long-term change in the wind field one may expect changes in the seasonal temperature variation as well. We therefore compare the residues of the annual amplitudes A_1 with those of σ_N (Figure 12). As mentioned before, they are anticorrelated (r = −0.63). The corresponding sensitivity is S_r = (−0.47 ± 0.11) K/K. Hence, there appears to be a substantial influence of the gravity waves on the harmonic amplitude.

[71] The long-term trends of the two parameters are opposite as well (Figures 9 and 12). They are, however, fairly flat and have large errors. In this case, a trend sensitivity S_t is not very meaningful.

[72] Changes of the seasonal temperature variation suggest changes of the summer duration. The Equivalent Summer Duration (ESD) is the time interval in Figure 1 when the harmonic fit curve is below 198 K. It varies from year to year and shows a long-term increase of 1.2 days/year since 1988 [*Offermann et al.*, 2010]. The mean ESD is about 150 days. Hence, the increase is about 0.8%/year. The corresponding change rate of σ_N given above is 0.32 K/year, i.e., 1.5%/year. Although no direct conclusions can be drawn from these numbers it is interesting to note that they are on the same order of magnitude.

[73] The summer length can also be defined as the time difference between the zonal wind turnaround in spring and autumn [see *Offermann et al.*, 2010]. The turnaround method is in principle to be preferred to the ESD method because it is more objective. The spring turnaround data in the mesosphere are available from the measurements at the station of Juliusruh. They show a trend of about 0.8 days/year toward earlier times (at 94 km [*Offermann et al.*, 2010, Figure 15]). This compares well with the change rate of the spring point of the ESD analysis of about 0.9 days/year [*Offermann et al.*, 2010]. This shows that the two definitions of summer length yield similar results. However, the autumn turnaround data of the wind station are not available for a period sufficiently long to derive a trend. Hence the turnaround method cannot be applied directly. We therefore use estimated reversal times as a surrogate as follows.

[74] A change of the spring/autumn time difference can be roughly estimated from the long-term increase of the zonal wind velocity U. The zonal wind U increases from spring turnaround toward the middle of summer, and subsequently decreases again toward autumn turnaround. This is sketched in a very simplified manner in Figure 14 by assuming linear changes (87.5 km). The summer length is 2*SL (see Figure 14). The parameter u denotes the increase of the wind speed (for instance in one year). It is assumed here for simplicity that u is the same at all times of the summer. This leads to a shift sl of the turnaround point (U = 0) to earlier times in the first half of summer. From the geometry of Figure 14 it follows that U_0/SL = u/sl. Mid summer maximum wind speed U_0 is about 12 m/s, half of the summer length is SL = 62 days (data for 87.5 km from *Offermann et al.* [2011, Figure 6]). The increase rate u as derived above from *Keuer et al.* [2007] is u = 0.52 (m/s)/year. The resulting increase of the summer length is sl = 2.7 days/year (shift of spring turnaround toward earlier times), which is half of the total increase.

[75] This estimate is based on the approximate finding that there is almost no change of wind speed in winter [*Keuer et al.*, 2007]. The estimate is an overestimation because it assumes the same trend during all of summer. This is an oversimplification as the real trend increases toward the middle of summer [*Keuer et al.*, 2007] which leads to smaller sl values. Comparing this to the results given above [*Offermann et al.*, 2010] our surrogate yields the right direction and the right order of magnitude. These results suggest a physical relationship of the increase of summer duration and the increases of gravity waves and zonal wind.

[76] It is interesting to note that very similar changes of spring turnaround as discussed here (but with opposite sign) have been reported from measurements and modeling of the stratosphere in the Northern as well as the Southern Hemisphere [*McLandress et al.*, 2010; *Offermann et al.*, 2010].

[77] It has been noted in the literature that gravity wave increases may lead to increased atmospheric instability in the mesosphere [*Hecht*, 2004]. Measured changes of barotropic and baroclinic instabilities have been reported by *Offermann et al.* [2011]. They find a modification of the occurrence distribution of the Quasi-Two Day Waves (QTDW) in the summer mesosphere. For instance, instability appears to have increased in recent years in the middle

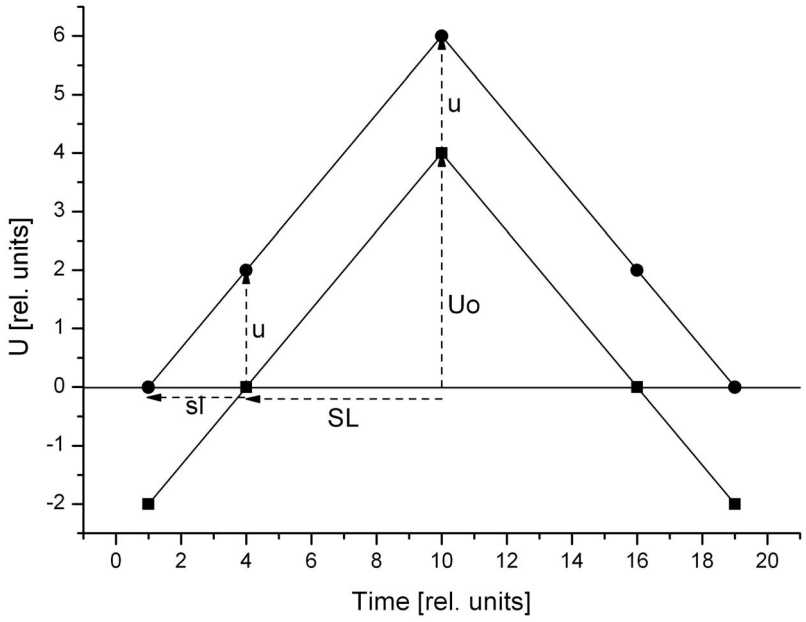

Figure 14. Sketch of zonal wind variation in summer (87.5 km; see text). Summer length is 2*SL. Increase of summer length is by 2*sl and results from an increase of zonal wind U by u.

of May and at the end of August (peaks of QTDW amplitudes, Offermann et al.'s Figure 12). These are times of substantial increases of our gravity wave proxy σ_N as shown in Figure 13. *Offermann et al.* [2011] also gave some quantitative estimate of the baroclinic instability in the mesosphere from radar wind measurements at Juliusruh. They found an increase especially in the early part of summer (DOY 100–140). The baroclinic instability increased by about a factor 1.6 (±6%) in seven years (using the intervals 1990–1995 and 1997–2002 for comparison, Offermann et al.'s Figure 13). This can be compared to our σ_N data in the same time interval (1993–2000). These increase by a factor 1.5 (±13%) according to the fit line in Figure 12. This is an interesting coincidence that suggests more detailed studies.

7. Summary and Conclusions

[78] Fluctuations of mesospheric temperature and winds have frequently been taken as proxies for atmospheric gravity waves. Here we use temperature standard deviations during the night (σ_N) as indicators of gravity wave activity. Hydroxyl (OH) temperature measurements at Wuppertal (51°N, 7°E) and Hohenpeissenberg (48°N, 11°E) are analyzed. Furthermore, data in windows of 21 min length are Fourier analyzed and yield oscillation amplitudes for periods between 3 and 10 min. These amplitudes are expressed by their equivalent standard deviation σ_a for comparison with σ_N. Standard deviations σ_a and σ_N are found closely correlated.

[79] The mean duration of the nightly measurements is approximately 5 h. Wave periods up to this length are therefore covered by σ_N. Hence, relatively short to very short waves/oscillations are analyzed here. The shortest periods (3 min) in their majority cannot be gravity waves as these mostly exist at periods longer than the Brunt-Väissällä period (5 min). They are therefore interpreted as "ripples" that result from atmospheric instabilities/gravity wave breaking. Parameter σ_a thus contains ripples and short-period gravity waves. There is a close correlation between the ripples (3 min amplitudes), σ_a, and σ_N. Therefore these parameters are taken here as proxies for gravity waves and breaking gravity waves. This is supported by a close relationship with turbulent eddy coefficients obtained from a general circulation model (WACCM 3.5). Hence, the picture suggested here is that gravity wave activity in general is accompanied by a certain amount of wave breaking/dissipation at the altitudes of our measurements. This leads us to use the standard deviations to study variations of the forcing of dynamics/circulation in the mesosphere.

[80] Time variations of σ_N (and σ_a, 3 min amplitudes) are observed on seasonal, intradecadal, and interdecadal (trend) scales. Seasonal variations show on the mean two relative maxima near (somewhat before) circulation turnaround in spring and autumn. This has been found in 13 years of Wuppertal data and in very similar form in several years of simultaneous measurements at Hohenpeissenberg. A similar seasonal variation has recently been obtained from a gravity wave analysis of SABER data. A physical relationship of gravity wave maxima and times of circulation reversal needs to be determined, though.

[81] There is an extradecadal (trend) variation of σ_N seen as a long-term increase (16 years). Similar variations are found in the zonal wind speed and the annual component A_1 of the seasonal temperature variation. The intradecadal changes as well as the extradecadal variations of the zonal wind closely correlate with the parameter σ_N.

[82] The long-term increase of σ_N is 1.5%/year, which means a corresponding increase of long-term gravity wave activity. This appears to lead to an increase of zonal wind speed of 0.5 m/s per year at 87.5 km altitude and 55°N. This trend value allows estimating a change in summer length at

the mesopause. An increase results that is in qualitative agreement with an increase of the Equivalent Summer Duration (ESD) reported in the literature.

[83] In summary, we observe changes of several dynamical parameters that appear compatible with considerable variations and a long-term increase of the activity of short-period gravity waves in the mesosphere.

[84] **Acknowledgments.** We thank Dan Marsh (ACD, NCAR, Boulder, Colorado) for making the mesospheric eddy coefficients of WACCM 3.5 available to us. Many helpful discussions with P. Hoffmann (IAP, Kühlungsborn) are gratefully acknowledged.

References

Alexander, M. J. (1998), Interpretation of observed climatological patterns in stratospheric gravity wave variance, *J. Geophys. Res.*, *103*, 8627–8640, doi:10.1029/97JD03325.

Alexander, M. J., and D. Ortland (2010), Equatorial waves in High Resolution Dynamics Limb Sounder (HIRDLS) data, *J. Geophys. Res.*, *115*, D24111, doi:10.1029/2010JD014782.

Andrews, D. G., J. R. Holton, and C. B. Leovy (1987), *Middle Atmosphere Dynamics*, *Int. Geophys. Ser.*, vol. 40, Academic, San Diego, Calif.

Beldon, C. L., and N. J. Mitchell (2009), Gravity waves in the mesopause region observed by meteor radar, 2: Climatologies of gravity waves in the Antarctic and Arctic, *J. Atmos. Sol. Terr. Phys.*, *71*, 875–884, doi:10.1016/j.jastp.2009.03.009.

Bittner, M., D. Offermann, H.-H. Graef, M. Donner, and K. Hamilton (2002), An 18-year time series of OH rotational temperatures and middle atmosphere decadal variations, *J. Atmos. Sol. Terr. Phys.*, *64*, 1147–1166, doi:10.1016/S1364-6826(02)00065-2.

Dewan, E. M., W. Pendleton, N. Grossbard, and P. Espy (1992), Mesospheric OH airglow temperature fluctuations: A spectral analysis, *Geophys. Res. Lett.*, *19*, 597–600, doi:10.1029/92GL00391.

Dowdy, A. J., R. A. Vincent, M. Tsutsumi, K. Igarashi, Y. Murayama, W. Singer, and D. J. Murphy (2007), Polar mesosphere and lower thermosphere dynamics: 1. Mean wind and gravity wave climatologies, *J. Geophys. Res.*, *112*, D17104, doi:10.1029/2006JD008126.

Eckermann, S. D., and P. Preusse (1999), Global measurements of stratospheric mountain waves from space, *Science*, *286*, 1534–1537, doi:10.1126/science.286.5444.1534.

Ern, M., P. Preusse, M. J. Alexander, and C. D. Warner (2004), Absolute values of gravity momentum flux derived from satellite data, *J. Geophys. Res.*, *109*, D20103, doi:10.1029/2004JD004752.

Eyring, V., T. G. Shepherd, and D. W. Waugh (Eds.) (2010), SPARC CCMVal report on the evaluation of chemistry-climate models, *SPARC Rep. 4*, SPARC, Univ. of Toronto, Toronto, Ont., Canada. [Available at http://www.atmosp.physics.utoronto.ca/SPARC.]

Fetzer, E. J., and J. C. Gille (1994), Gravity wave variances in LIMS temperatures, I, Variability and comparison with background winds, *J. Atmos. Sci.*, *51*, 2461–2483, doi:10.1175/1520-0469(1994)051<2461:GWVILT>2.0.CO;2.

Fritts, D. C., and M. J. Alexander (2003), Gravity wave dynamics and effects in the middle atmosphere, *Rev. Geophys.*, *41*(1), 1003, doi:10.1029/2001RG000106.

Fritts, D. C., S. L. Vadas, K. Wan, and J. A. Werne (2006), Mean and variable forcing of the middle atmosphere by gravity waves, *J. Atmos. Sol. Terr. Phys.*, *68*, 247–265, doi:10.1016/j.jastp.2005.04.010.

Fritts, D. C., L. Wang, and J. Werne (2009), Gravity wave-fine structure interactions: A reservoir of small-scale and large scale turbulence energy, *Geophys. Res. Lett.*, *36*, L19805, doi:10.1029/2009GL039501.

Garcia, R. R., D. R. Marsh, D. E. Kinnison, B. A. Boville, and F. Sassi (2007), Simulation of secular trends in the middle atmosphere, 1950–2003, *J. Geophys. Res.*, *112*, D09301, doi:10.1029/2006JD007485.

Geller, M. A., and J. Gong (2010), Gravity wave kinetic, potential, and vertical fluctuation energies as indicators of different frequency gravity waves, *J. Geophys. Res.*, *115*, D11111, doi:10.1029/2009JD012266.

Hecht, J. H. (2004), Instability layers and airglow imaging, *Rev. Geophys.*, *42*, RG1001, doi:10.1029/2003RG000131.

Hecht, J. H., S. K. Ramsay Howat, R. L. Walterscheid, and J. R. Isler (1995), Observations of spectra of intensity fluctuations of the OH Meinel nightglow during ALOHA-93, *Geophys. Res. Lett.*, *22*, 2873–2876, doi:10.1029/95GL03020.

Hecht, J. H., A. Z. Liu, R. L. Walterscheid, and R. J. Rudy (2005), Maui Mesosphere and Lower Thermosphere (Maui MALT) observations of the evolution of Kelvin-Helmholtz billows formed near 86 km altitude, *J. Geophys. Res.*, *110*, D09S10, doi:10.1029/2003JD003908.

Hecht, J. H., A. Z. Liu, R. L. Walterscheid, S. J. Franke, R. J. Rudy, M. J. Taylor, and P.-D. Pautet (2007), Characteristics of short-period wavelike features near 87 km altitude from airglow and lidar observations over Maui, *J. Geophys. Res.*, *112*, D16101, doi:10.1029/2006JD008148.

Hines, C. O. (1960), Internal atmospheric gravity waves at ionospheric heights, *Can. J. Phys.*, *38*, 1441–1481, doi:10.1139/p60-150.

Hoffmann, P., M. Rapp, W. Singer, and D. Keuer (2011), Trends of mesospheric gravity waves at northern middle latitudes during summer, *J. Geophys. Res.*, doi:10.1029/2011JD015717, in press.

Holton, J. R. (1983), The influence of gravity wave breaking on the general circulation of the middle atmosphere, *J. Atmos. Sci.*, *40*, 2497–2507, doi:10.1175/1520-0469(1983)040<2497:TIOGWB>2.0.CO;2.

Horinouchi, T., T. Nakamura, and J. Kosaka (2002), Convectively generated mesoscale gravity waves simulated throughout the middle atmosphere, *Geophys. Res. Lett.*, *29*(21), 2007, doi:10.1029/2002GL016069.

Jacobi, C., N. M. Gavrilov, D. Kürschner, and K. Fröhlich (2006), Gravity wave climatology and trends in the mesosphere/lower thermosphere region deduced from low-frequency drift measurements 1984–2003 (52.1°N, 13.2°E), *J. Atmos. Sol. Terr. Phys.*, *68*, 1913–1923, doi:10.1016/j.jastp.2005.12.007.

Jiang, J. H., S. D. Eckermann, D. L. Wu, and D. Y. Wang (2006), Interannual variation of gravity waves in the Arctic and Antarctic winter middle atmosphere, *Adv. Space Res.*, *38*, 2418–2423, doi:10.1016/j.asr.2005.09.036.

Keuer, D., P. Hoffmann, W. Singer, and J. Bremer (2007), Long-term variations of the mesospheric wind field at mid-latitudes, *Ann. Geophys.*, *25*, 1779–1790, doi:10.5194/angeo-25-1779-2007.

Krebsbach, M., and P. Preuße (2007), Comparison of global distributions of zonal mean gravity wave variance inferred from different satellites measurements, *Geophys. Res. Lett.*, *34*, L03814, doi:10.1029/2006GL028040.

Laštovička, J. (2009), Global pattern of trends in the upper atmosphere and ionosphere: Recent progress, *J. Atmos. Sol. Terr. Phys.*, *71*, 1514–1528, doi:10.1016/j.jastp.2009.01.010.

Laštovička, J., R. A. Akmaev, G. Beig, J. Bremer, J. T. Emmert, C. Jacobi, M. J. Jarvis, G. Nedoluha, Y. I. Portnyagin, and T. Ulich (2008), Emerging pattern of global change in the upper atmosphere and ionosphere, *Ann. Geophys.*, *26*, 1255–1268, doi:10.5194/angeo-26-1255-2008.

Laštovička, J., P. Krizan, and M. Kozubek (2010), Long-term trends in the middle atmosphere dynamics at northern middle latitudes—One regime or two different regimes?, *Atmos. Chem. Phys. Discuss.*, *10*, 2633–2668, doi:10.5194/acpd-10-2633-2010.

Li, F., A. Z. Liu, G. R. Swenson, J. H. Hecht, and W. A. Robinson (2005), Observation of gravity wave breakdown into ripples associated with dynamical instabilities, *J. Geophys. Res.*, *110*, D09S11, doi:10.1029/2004JD004849.

Liu, G., G. G. Shepherd, and R. G. Roble (2008), Seasonal variations of the nighttime O(^{1}S) and OH airglow emission rate at mid-to-high latitudes in the context of the large- scale circulation, *J. Geophys. Res.*, *113*, A06302, doi:10.1029/2007JA012854.

Manson, A. H., C. E. Meek, C. Hall, W. K. Hocking, J. MacDougall, S. Franke, K. Igarashi, D. Riggin, D. C. Fritts, and R. A. Vincent (1999), Gravity wave spectra, directions and wave interactions: Global MLT-MFR network, *Earth Planets Space*, *51*, 543–562.

McLandress, C., M. J. Alexander, and D. L. Wu (2000), Microwave Limb Sounder observations of gravity waves in the stratosphere: A climatology and interpretation, *J. Geophys. Res.*, *105*, 11,947–11,967, doi:10.1029/2000JD900097.

McLandress, C., A. I. Jonsson, D. A. Plummer, M. C. Reader, J. F. Sinocca, and T. G. Shepherd (2010), Separating the dynamical effects of climate change and ozone depletion. Part I: Southern Hemisphere stratosphere, *J. Clim.*, *23*, 5002–5020, doi:10.1175/2010JCLI3586.1.

Medeiros, A. F., H. Takahashi, R. A. Buriti, J. Fechine, C. M. Wrasse, and D. Gobbi (2007), MLT gravity wave climatology in the South America equatorial region observed by airglow imager, *Ann. Geophys.*, *25*, 399–406, doi:10.5194/angeo-25-399-2007.

Morgenstern, O., et al. (2010), Review of the formulation of present-generation stratospheric chemistry-climate models and associated forcings, *J. Geophys. Res.*, *115*, D00M02, doi:10.1029/2009JD013728.

Mulligan, F. J., M. E. Dyrland, F. Sigernes, and C. S. Deehr (2009), Inferring hydroxyl layer peak heights from ground-based measurements of OH(6–2) band integrated emission rate at Longyearbyen (78°N, 16°E), *Ann. Geophys.*, *27*, 4197–4205, doi:10.5194/angeo-27-4197-2009.

Nakamura, T., A. Higashikawa, T. Tsuda, and Y. Matsushita (1999), Seasonal variations of gravity wave structures in OH airglow with a CCD imager at Shigaraki, *Earth Planets Space*, *51*, 897–906.

Nakamura, T., T. Aono, T. Tsuda, A. G. Admiranto, E. Achmad, and Suranto (2003), Mesospheric gravity waves over a tropical convective region observed by OH airglow imaging in Indonesia, *Geophys. Res. Lett.*, *30*(17), 1882, doi:10.1029/2003GL017619.

Nielsen, K., M. J. Taylor, R. E. Hibbins, and M. J. Jarvis (2009), Climatology of short-period mesospheric gravity waves over Halley, Antarctica (76°S, 27°W), *J. Atmos. Sol. Terr. Phys.*, *71*, 991–1000, doi:10.1016/j.jastp.2009.04.005.

Oberheide, J., D. Offermann, J. M. Russell III, and M. G. Mlynczak (2006), Intercomparison of kinetic temperature from 15 μm CO_2 limb emissions and OH*(3,1) rotational temperature in nearly coincident air masses: SABER, GRIPS, *Geophys. Res. Lett.*, *33*, L14811, doi:10.1029/2006GL026439.

Offermann, D., M. Jarisch, M. Donner, W. Steinbrecht, and A. I. Semenov (2006), OH temperature re-analysis forced by recent variance increases, *J. Atmos. Sol. Terr. Phys.*, *68*, 1924–1933, doi:10.1016/j.jastp.2006.03.007.

Offermann, D., M. Jarisch, H. Schmidt, J. Oberheide, K. U. Grossmann, O. Gusev, J. M. Russell III, and M. G. Mlynczak (2007), The "wave turbopause," *J. Atmos. Sol. Terr. Phys.*, *69*, 2139–2158, doi:10.1016/j.jastp.2007.05.012.

Offermann, D., O. Gusev, M. Donner, J. M. Forbes, M. Hagan, M. G. Mlynczak, J. Oberheide, P. Preusse, H. Schmidt, and J. M. Russell III (2009), Relative intensities of middle atmosphere waves, *J. Geophys. Res.*, *114*, D06110, doi:10.1029/2008JD010662.

Offermann, D., P. Hoffmann, P. Knieling, R. Koppmann, J. Oberheide, and W. Steinbrecht (2010), Long-term trends and solar cycle variations of mesospheric temperature and dynamics, *J. Geophys. Res.*, *115*, D18127, doi:10.1029/2009JD013363.

Offermann, D., P. Hoffmann, P. Knieling, R. Koppmann, J. Oberheide, D. M. Riggin, V. M. Tunbridge, and W. Steinbrecht (2011), Quasi 2 day waves in the summer mesosphere: Triple structure of amplitudes and long-term development, *J. Geophys. Res.*, *116*, D00P02, doi:10.1029/2010JD015051.

Pautet, P.-D., M. J. Taylor, A. Z. Liu, and G. R. Swenson (2005), Climatology of short-period gravity waves observed over northern Australia during the Darwin Area Wave Experiment (DAWEX) and their dominant source regions, *J. Geophys. Res.*, *110*, D03S90, doi:10.1029/2004JD004954.

Placke, M., G. Stober, and C. Jacobi (2010), Gravity wave momentum fluxes in the MLT–Part I: Seasonal variation at Collm (51.3°N, 13.0°E), *J. Atmos. Sol. Terr. Phys.*, *73*, 904–910, doi:10.1016/j.jastp.2010.07.012.

Placke, M., P. Hoffmann, E. Becker, Ch. Jacobi, W. Singer, and M. Rapp (2011), Gravity wave momentum fluxes in the MLT–Part II: Meteor radar investigations at high and midlatitudes in comparison with modeling studies, *J. Atmos. Sol. Terr. Phys.*, *73*, 911–920, doi:10.1016/j.jastp.2010.05.007.

Portnyagin, Y. I., E. G. Merzlyakov, T. V. Solovjova, C. Jacobi, D. Kürschner, A. Manson, and C. Meek (2006), Long-term trends and year-to-year variability of mid-latitude mesosphere/lower thermosphere winds, *J. Atmos. Sol. Terr. Phys.*, *68*, 1890–1901, doi:10.1016/j.jastp.2006.04.004.

Preusse, P., et al. (2006), Tropopause to mesopause gravity waves in August: Measurement and modeling, *J. Atmos. Sol. Terr. Phys.*, *68*, 1730–1751, doi:10.1016/j.jastp.2005.10.019.

Preusse, P., S. D. Eckermann, and M. Ern (2008), Transparency of the atmosphere to short horizontal wavelength gravity waves, *J. Geophys. Res.*, *113*, D24104, doi:10.1029/2007JD009682.

Preusse, P., S. D. Eckermann, M. Ern, J. Oberheide, R. H. Picard, R. G. Roble, M. Riese, J. M. Russell III, and M. G. Mlynczak (2009), Global ray tracing simulations of the SABER gravity wave climatology, *J. Geophys. Res.*, *114*, D08126, doi:10.1029/2008JD011214.

Rapp, M., B. Strelnikov, A. Müllemann, and F.-J. Lübken (2004), Turbulence measurements and implications for gravity wave dissipation during the MaCWAVE/MIDAS rocket program, *Geophys. Res. Lett.*, *31*, L24S07, doi:10.1029/2003GL019325.

Richter, J. H., F. Sassi, and R. R. Garcia (2010), Toward a physically based gravity wave source parameterization in a general circulation model, *J. Atmos. Sci.*, *67*, 136–156, doi:10.1175/2009JAS3112.1.

Savitzky, A., and M. J. E. Golay (1964), Smoothing and differentiation of data by simplified least squares procedures, *Anal. Chem.*, *36*, 1627–1639, doi:10.1021/ac60214a047.

Scheer, J., E. R. Reisin, O. Gusev, W. J. R. French, G. Hernandez, R. Huppi, P. Ammosov, G. A. Gavrilyeva, and D. Offermann (2006), Use of CRISTA mesopause region temperatures for the intercalibration of ground-based instruments, *J. Atmos. Sol. Terr. Phys.*, *68*, 1698–1708, doi:10.1016/j.jastp.2005.12.009.

Shiokawa, K., Y. Otsuka, and T. Ogawa (2009), Propagation characteristics of nighttime mesospheric and thermospheric waves observed by optical mesosphere thermosphere imagers at middle and low latitudes, *Earth Planets Space*, *61*, 479–491.

Simkhada, D. B., J. B. Snively, M. J. Taylor, and S. J. Franke (2009), Analysis and modeling of ducted and evanescent gravity waves observed in the Hawaiian airglow, *Ann. Geophys.*, *27*, 3213–3224, doi:10.5194/angeo-27-3213-2009.

Snively, J. B., V. P. Pasko, and M. J. Taylor (2010), OH and OI airglow modulation by ducted short-period gravity waves: Effects of trapping altitude, *J. Geophys. Res.*, *115*, A11311, doi:10.1029/2009JA015236.

Suzuki, S., K. Shiokawa, K. Hosokawa, K. Nakamura, and W. K. Hocking (2009), Statistical characteristics of polar cap mesospheric gravity waves observed by an all-sky airglow imager at Resolute Bay, Canada, *J. Geophys. Res.*, *114*, A01311, doi:10.1029/2008JA013652.

Taylor, M. J., and M. A. Hapgood (1990), On the origin of ripple-type wave structure in the OH nightglow emission, *Planet. Space Sci.*, *38*, 1421–1430, doi:10.1016/0032-0633(90)90117-9.

Taylor, M. J., W. R. Pendleton Jr., S. Clark, H. Takahashi, D. Gobbi, and R. A. Goldberg (1997), Image measurements of short-period gravity waves at equatorial latitudes, *J. Geophys. Res.*, *102*, 26,283–26,299, doi:10.1029/96JD03515.

Taylor, M. J., W. R. Pendleton, P.-D. Pautet, Y. Zhao, C. Olsen, H. K. Surendra Babu, A. F. Medeiros, and H. Takahashi (2007), Recent progress in mesospheric gravity wave studies using nightglow imaging system, *Rev. Bras. Geofis.*, *25*, suppl. 2, 49–58, doi:10.1590/S0102-261X2007000600007.

Wu, D. L., and J. W. Waters (1996), Gravity-wave-scale temperature fluctuations seen by the UARS MLS, *Geophys. Res. Lett.*, *23*, 3289–3292, doi:10.1029/96GL02924.

Wu, D. L., P. Preusse, S. D. Eckermann, J. H. Jiang, M. de la Torre Juarez, L. Coy, and D. Y. Wang (2006), Remote sounding of atmospheric gravity waves with satellite limb and nadir techniques, *Adv. Space Res.*, *37*, 2269–2277, doi:10.1016/j.asr.2005.07.031.

Yang, G., B. Clemesha, P. Batista, and D. Simonich (2010), Seasonal variations of gravity wave activity and spectra derived from sodium temperature lidar, *J. Geophys. Res.*, *115*, D18104, doi:10.1029/2009JD012367.

Yue, J., T. Nakamura, C.-Y. She, M. Weber, W. Lyons, and T. Li (2010), Seasonal and local time variability of ripples from airglow imager observations in US and Japan, *Ann. Geophys.*, *28*, 1401–1408, doi:10.5194/angeo-28-1401-2010.

C. Kalicinsky, P. Knieling, R. Koppmann, D. Offermann, and J. Wintel, Physics Department, Wuppertal University, Gauss-Strasse 20, D-42097 Wuppertal, Germany. (offerm@uni-wuppertal.de)

W. Steinbrecht, Meteorologisches Observatorium, D-82383 Hohenpeissenberg, Germany.